

Electronic Phase Propagation Speed in BaFe₂As₂ Revealed by Dilatometry

Xin Qin,^{1,2} Xingyu Wang,³ Wenshan Hong,^{1,2} Mengqiao Geng,^{1,2}
Yuan Li,^{1,2} Huiqian Luo,³ Shiliang Li,³ and Yang Liu^{1,2,*}

¹*International Center for Quantum Materials, Peking University, Haidian, Beijing 100871, China*

²*Hefei National Laboratory, Hefei 230088, China*

³*Beijing National Laboratory for Condensed Matter Physics,
Institute of Physics, Chinese Academy of Sciences, Beijing 100190, China*

(Dated: March 27, 2024)

Thermal expansion offers deep insights into phase transitions in condensed matter physics. Utilizing an advanced AC-temperature dilatometer with picometer resolution, this study clearly resolves the antiferromagnetic and structural transition in BaFe₂As₂. The implementation of temperature oscillation reveals a hysteresis near the transition temperature T_N with unprecedented resolution. Unexpectedly, we find that the hysteretic width exhibits a universal dependence on the parameters of temperature oscillation and the sample's longitudinal dimension, which in turn reveals a finite transition speed. Our quantitative analysis shows that this phase boundary propagates at a mere 188 $\mu\text{m/s}$ – a speed seven orders of magnitude slower than acoustic waves. It suggests a hidden thermodynamic constraint imposed by the electronic degrees of freedom. Our research not only sheds light on the dynamics of phase transitions between different correlated phases, but also establishes high precision dilatometry as a powerful tool for material studies. This measurement technique, when properly modified, can be extended to studies of other material properties such as piezoelectric, magneto-restriction, elastic modulus, etc.

I. INTRODUCTION

Phase transitions are of great interest in study of materials, where a variety of degrees of freedom are often coupled together. It is important to experimentally differentiate closely related transitions, as well as to identify the primary driving force behind transition. Because density is a true scalar that remains invariant under all symmetry operations relevant to solids, it is expected to have symmetry-allowed coupling to all phase transitions. As a result, accurately measured density can be used for detection and classification of phase transitions. In practice, this is often done with length measurements such as the linear thermal expansion coefficient α [1–6]. Along with atomic microscope piezocantilever, strain gauge, piezobender and X-ray diffraction[7–10], the mostly used and accurate dilatometer is based on plate capacitors. The length change of the sample ΔL is captured through monitoring the capacitance between the sample's upper surface and a metal reference surface, and α is deduced by numerical differentiation $\alpha = L^{-1}dL/dT$ [11–16]. Unfortunately, the sample is always at equilibrium, because this method needs an ultra-high temperature uniformity of the whole mechanical structure to achieving its high accuracy, and its capacitance measurement limits temperature varying speed to $\sim 10^{-3}$ K/s.

In condensed matter physics, the dynamic behavior of transitions is always attractive and many techniques have been implemented [17–21]. Limited either by resolution or slow response, conventional dilatometers are not capable in studying the dynamic procedure of phase transi-

tions. In this work, we present a new approach of measuring thermal expansion with pm-resolution using optical interferometers. Using oscillating temperature, we can analyze the dynamic response of the thermal expansion in the frequency domain. As a demonstration, we examine the anti-ferromagnetism phase transitions in BaFe₂As₂ [22–25]. Our systematic investigation reveals a hysteresis that originates from the nonequilibrium state of sample near the transition temperature T_N . The width of the hysteresis in temperature is proportional to the sample thickness L , the frequency and amplitude of temperature oscillation δT . Thanks to the continuous perturbation by δT , this hysteresis is likely a manifestation of the fact that the phase transitions is not infinitely sharp in time and the phase boundary propagates with a finite speed. The measured speed $\simeq 188 \mu\text{m/s}$ is significantly smaller than the acoustic velocity, shining light on the complex nature of domain boundary dynamics.

II. EXPERIMENTAL SETUP

We use BaFe₂As₂, the parent compound of the “122” Fe-based superconductors, an ideal prototypical example of phase transition(s) with coupled degrees of freedom, for demonstration. It is generally believed to have a two-step phase transition when temperature reduces [22–25], i.e. a second-order structural transition at $T_S = 134.5$ K followed by a first-order magnetic transition at $T_N = 133.75$ K [26, 27]. An electronic nematic phase is reported between T_S and T_N [28–32]. We study four single-crystal as grown samples (S1 to S4) with typically in-plane size as $(2\sim 4) \times (2\sim 4)$ mm² and different thickness $L = 430, 210, 400$ and $75 \mu\text{m}$, respectively. Sample S1 and S2 are cleaved from the same piece, while S3 and S4 come from

* liuyang02@pku.edu.cn

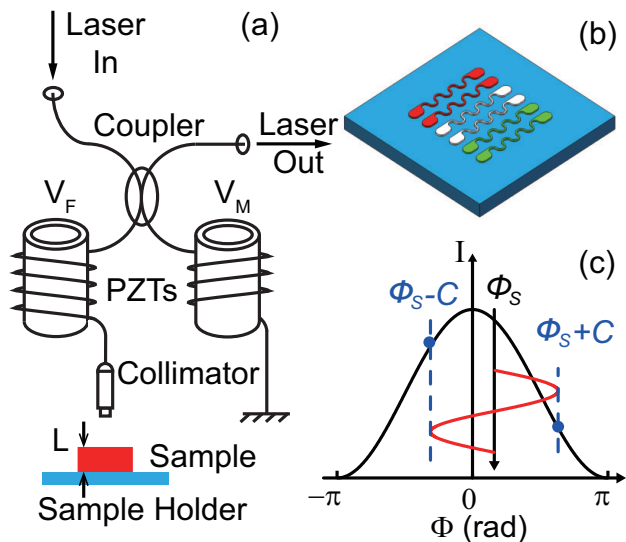


FIG. 1. (a) Our dilatometer implements a fiber Michelson interferometer. The probing (left) and reference (right) arms are wound around cylindrical PZT rings by which we can tune their length using the modulation and feedback voltages V_M and V_F . V_M generate a phase modulation $\phi_M = C \cos(\omega_M t)$, and V_F eliminates the thermal drift $\Phi_0 \approx 0$. (b) A detailed cartoon of the sapphire sample holder. The white, red and green meadow Pt wires are used as thermometer, AC and DC heaters. (c) The interfered light intensity $I = \cos(\Phi)$ is an odd function of the two beams' phase difference $\Phi = \Phi_M + \phi_S$, where ϕ_S originates from the thermal expansion induced by the AC temperature oscillation. Φ oscillates between $\phi_S \pm C$ and the optical power difference between the two Φ extremes has a positive dependence on ϕ_S ; see text for detailed description of our measurement principle.

another one.

The samples are placed on upper surface of sapphire sample holder with extremely thin ($\sim 5\mu\text{m}$) N-Grase for better thermal conductivity so they are considered to be free-standing and the thermal expansion is measured along their c -axis direction. There are three pairs of evaporated Pt wires on the lower surface of sample holder which are used as thermometer, AC and DC heaters, respectively; see Fig. 1(b). We measure the thermometer resistance and calibrate it by the cryostat temperature when the heaters are switched off. The real-time sample temperature can be separated into a slowly sweeping DC part T_0 by DC heater and an AC oscillation δT by AC heater. δT of sample induces an oscillation δL in sample thickness and then the thermal expansion coefficient α can be deduced by $\alpha = L^{-1}\delta L/\delta T$ with the measurements of δL and δT by lock-in technique. We are able to achieve performance comparable to the best reported capacitive dilatometry[16], i.e. pm-resolution in δL amplitude $\langle \delta L \rangle$ and mK-resolution in δT amplitude $\langle \delta T \rangle$, with dynamics measurement nature.

The δL measurement of our dilatometer is based on a high resolution optical fiber Michelson interferometer

with and the output interference light intensity I depends on the phase difference Φ between probing and reference light beam as $I = I_0[1 + \cos(\Phi)]$. We can tune the optical length of the two beams by applying the modulation and feedback voltages, V_M and V_F , to the corresponding PZT rings; see Fig. 1(a). Φ consists three different components: the modulation phase $\phi_M = C \cos(2\pi f_M t) \propto V_M$, the AC phase signal $\phi_S = 4\pi/\lambda \cdot \delta L$ where $\delta L = \alpha L \delta T$ is the sample's thermal expansion induced by AC temperature oscillation δT , and the slowly varying ϕ_0 caused by the thermal drift. C and f_M are the amplitude and frequency of the modulation, α is the thermal expansion coefficient and $\lambda = 1550 \text{ nm}$ is the optical wavelength. We compensate the thermal drift using the feedback voltage V_F so that ϕ_0 can be neglected. According to the Jacobi-Anger expansion, the amplitudes of the output optical power's 1st and 2nd harmonic component at f_M and $2f_M$ are $I_1 = I_0 J_1(C) \sin(\phi_S(t))$ and $I_2 = I_0 J_2(C) \cos(\phi_S(t))$, respectively; J_N is Bessel function of the N -th order. We measure I_1 & I_2 using lock-in technique to deduce the sample's thermal expansion through

$$\delta L = \frac{\lambda}{4\pi} \tan^{-1} \left(\frac{J_2(C)I_1}{J_1(C)I_2} \right) \approx \frac{J_2(C)\lambda}{4\pi J_1(C)I_2} \cdot I_1$$

The phase modulation frequency f_M is typically a few kHz, the AC temperature oscillation frequency f_S is 100 and 250 mHz, the feedback eliminates drifts at $\lesssim 0.1 \text{ Hz}$, and the T_0 sweeping rate is 10^{-4} K/s . Our resolution of $\langle \delta L \rangle$ is as small as about 5 pm when using 50 mHz resolution bandwidth, so that we can use $\langle \delta T \rangle$ as small as 5 mK, see Fig. 3. You can find more details about the design, principle and performance of our dilatometer in Ref. [33] if you're interested.

III. EXPERIMENTAL RESULTS

Fig. 2(a) shows typically measured δT and δL oscillations ($T_0 \simeq 130 \text{ K}$). The phase of these two oscillations are perfectly aligned, leading to a linear line in Fig. 2(b) whose slope is the thermal expansion coefficient α . α can be measured using lock-in technique by separating δL oscillation into in-phase and out-of-phase components in reference to δT . The in-phase component of α is finite and its out-of-phase component remains nearly zero at temperatures away from T_N , i.e. $T > 136.5 \text{ K}$ or $T < 135 \text{ K}$, suggesting that the sample is at equilibrium and have uniform phase. Besides the AC differential measurement of α , we can also measure the sample's DC thickness change directly from the feedback voltage V_F through $\Delta L = G V_F$, where $G = |\lambda/\pi \cdot d\Phi/dV_F|$ is the feedback gain.

In Fig. 2(c), ΔL taken from sample S1 ($L \simeq 430\mu\text{m}$) exhibits a jump of about $\Delta L/L \simeq 1.5 \times 10^{-4}$ at $T_N = 135.67 \text{ K}$ where the in-phase component of α has a huge negative peak. This first-order phase transition is consistent with our characterization of resistivity showed in left inset in Fig. 2(c) and previous reports that the sample

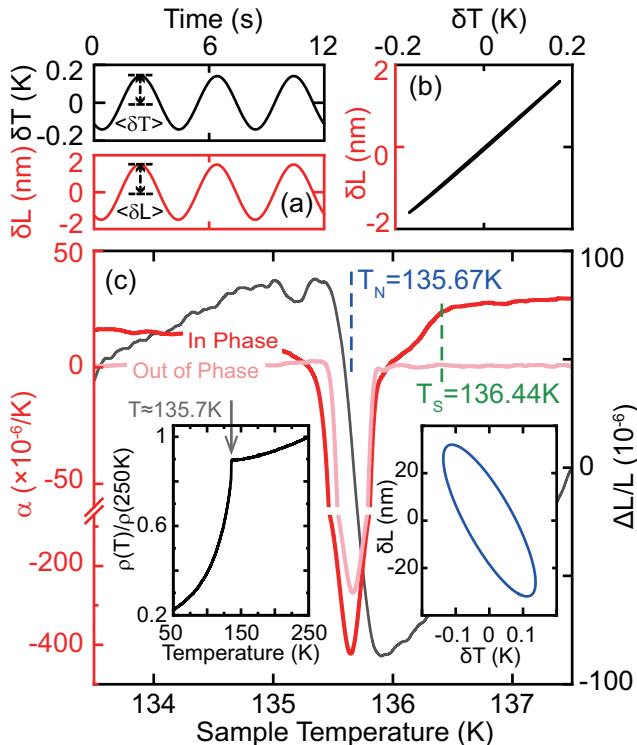


FIG. 2. (a) The typical δL and δT oscillations measured at $T_0 \simeq 130$ K. (b) The $\delta L/L$ vs. δT plot of panel (a) data. (c) The in-phase (red) and out-of-phase (pink) thermal expansion coefficient α by comparing δL and δT oscillations. The DC thickness variation ΔL (black) is deduced by $G \cdot V_F$. Data measured from sample S1 using δT frequency $f_S = 250$ mHz and amplitude $\langle \delta T \rangle = 0.14$ K. The magnetic transition temperature T_N and structural transition temperature T_S are marked by blue and green dash lines, respectively. The left inset is the zero-field normalized resistivity in (ab) plane and the right inset illustrates the δL vs. δT hysteresis loop at $T = T_N$.

makes a transition from a high-temperature PM phase to a low-temperature AFM phase [26]. Unlike the smooth and gradual increase on the low temperature side of T_N , α exhibit a clear kink in Fig. 2(c) at $T_S \simeq 136.44$ K, signaling the second order phase transition. This is consistent with the work by M. G. Kim *et al.* where a structural transition from tetragonal to orthorhombic lattice is observed by high resolution X-ray diffraction studies [26].

The small $\langle \delta T \rangle$ provides high resolution in temperature and reveals many features near the phase transition. Fig. 3 shows α measured from sample S2 ($L \simeq 210 \mu\text{m}$) where $\langle \delta T \rangle$ is as small as 5 and 10 mK. The α peak of the S2 data is narrow and deep, evidencing the sample's high quality since most of its bulk have the same T_N . The temperature resolutions are about 10mK and 20mK and both of them are smaller than the detailed features of the α peak. Clear kinks in α appear at a temperature T_S about 0.8 K above T_N , similar to sample S1, evidencing

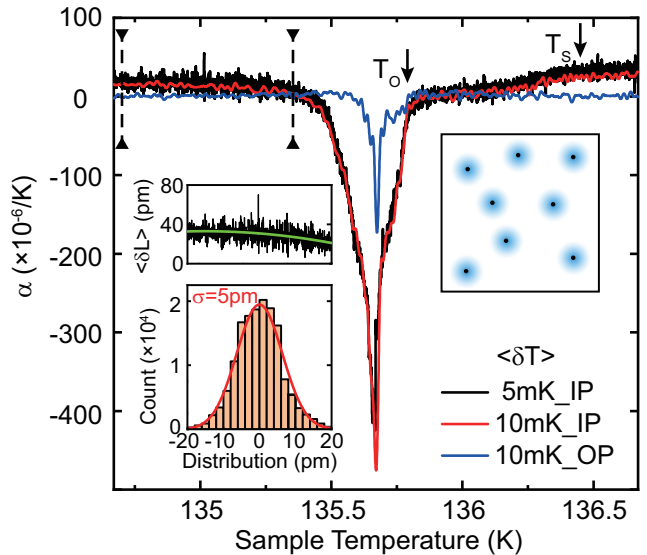


FIG. 3. α measured using extremely small $\langle \delta T \rangle = 5$ mK and 10 mK at 250 mHz from S2 (IP and OP are in-phase and out-of-phase part of α , respectively). The abrupt α drop at $T_O \simeq T_N + 0.1$ K suggests the formation of the AFM domains (blue dots) in the PM bath, illustrated by the right inset cartoon. The black dots represent the condensation nuclei of AFM domains, which might be defects. The left inset shows the measured $\langle \delta L \rangle$ in the range marked by the two vertical bars using 50 mHz resolution bandwidth. We deduce 5 pm resolution from the histogram of $\langle \delta L \rangle$ noise by subtracting the fitted green curve.

a strong link between these two transitions. Besides, we notice an extra abrupt change of α at $T_O \simeq T_N + 0.1$ K, which can be qualitative explained by the formation of AFM clusters around condensation nuclei such as defects while the substantial part of the sample remains PM, see the Fig. 3 inset [31].

Interestingly, the phase of δL and δT oscillation is no longer aligned near T_N , signaled by the large out-of-phase component of α in Fig 2 and Fig 3. In another word, δL vs. δT exhibits a hysteric ellipse, as shown Fig. 2(c) right inset. We choose the data of sample S1 at $f_S = 100$ mHz and $\langle \delta T \rangle \simeq 0.25$ K as an example and sum the DC component ΔL , induced by DC temperature T_0 sweeping and measured by V_F , and the AC component δL , induced by AC temperature change δT and measured by lock-in technique, as the real-time thickness of sample $\Delta L + \delta L$ and plot it as a function of the real-time temperature $T_0 + \delta T$ with black dots in Fig. 4(a). We highlight the relationship between $\Delta L + \delta L$ and $T_0 + \delta T$ within the one period of δT at $T_0 = T_N$ with red line and all the real-time thickness dots at phase transition region fall inside the area enclosed by this red line. The clear square hysteresis loop indicates that the sample is off-equilibrium and has two coexisting phases at the transition.

A detailed and accurate description of this hysteresis involves the dynamic process of the phase transi-

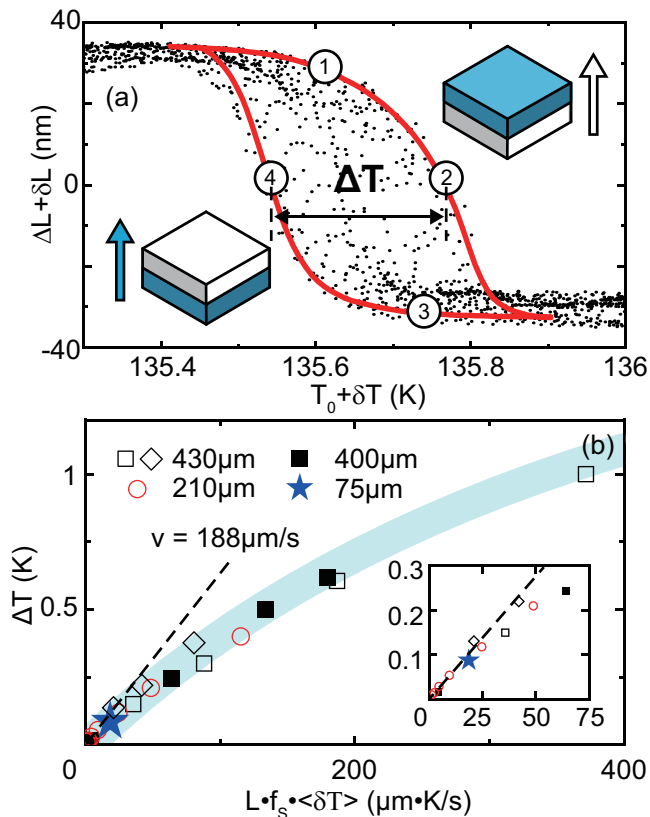


FIG. 4. (a) The thickness-temperature hysteresis. Data measured using $f_S = 100$ mHz and $\langle\delta T\rangle = 0.25$ K. Note that the peak-to-peak amplitude of temperature oscillation is $2\langle\delta T\rangle = 0.5$ K. We highlight one thermal cycle with thick red line and mark four positions in the loop. The inset cartoons illustrate the coexistence of the PM (white) and AFM (blue) phases and the propagation of their phase boundary. (b) Summarized ΔT vs. $L \cdot f_S \langle\delta T\rangle$ measured from different samples. We use $f_S = 100$ (open diamond) and 250 mHz (open square) for sample S1 data, and $f_S = 250$ mHz for all other data. The uncertainty of is comparable to the symbol size. The inset is a zoom-in plot near zero.

tion which is rather complicated and beyond the scope of this article. Fortunately, we can understand the observed phenomenon using a simple toy model. In Fig. 4(a) we highlight one thermal loop with red line and the four numbers mark four different conditions. The sample starts from a uniform AFM phase at low temperature. When the temperature increases through T_N at spot 1, the PM phase appears at the sample’s bottom surface which is thermally anchored to the sample holder. The PM domain grows and the phase boundary propagates upward until it reaches the samples’ top surface. When we cool the sample back through T_N at spot 3, the AFM phase forms at the sample bottom and grows upward. We can identify two specific positions labeled 2 and 4 in Fig. 4(a), which correspond to the midway of the phase transition. At these two points, the sample is divided half-and-half into AFM and PM phases, see the

inset cartoons. We define the distance between the two points, $\Delta T \approx 0.22$ K, as the width of the hysteresis loop.

It is worthwhile to mention several facts about ΔT . Firstly, the hysteresis width is not limited by the range of temperature oscillation, i.e. its the peak-to-peak amplitude $2\langle\delta T\rangle$. For example, $\Delta T \approx 0.22$ K in Fig. 4(a) is about 40% of $2\langle\delta T\rangle \approx 0.5$ K. This ratio becomes even smaller with slower frequency or thinner sample. Secondly, in contrast with systems such as supercooled pristine water which has liquid configuration well below its crystallization temperature if cooled slowly [34], the finite-width hysteresis loop is only because the temperature is changing “too fast” for this phase transition. ΔT vanishes when the amplitude or the frequency of δT approaches zero. The ratio of out-of-phase part and in-phase part of α can symbolize ΔT qualitatively. So the extremely narrow peak of out-of-phase part of α at $\langle\delta T\rangle = 10$ mK showed in Fig. 3 comparing the width peak at $\langle\delta T\rangle = 0.14$ K showed in Fig. 2(c) also indicates the transition becomes infinitely sharp if we sweep the AC temperature change sufficiently slow, which is consistent with previous capacitive dilatometry studies where no hysteresis is seen.

We measure the hysteresis loop from different samples using different δT frequencies f_S and amplitudes $\langle\delta T\rangle$. We use $f_S = 100$ and 250 mHz to measure S1, and $f_S = 250$ mHz for the other samples. We find that ΔT is proportional to the sample thickness L , the AC temperature oscillation frequency f_S and amplitude $\langle\delta T\rangle$. We summarize ΔT as a function of $L \cdot f_S \langle\delta T\rangle$ in Fig. 4(b). It is quite remarkable that all data points collapse onto the same curve highlighted by the blue band. We note that the phase boundary propagates by a distance $L/2$ to the midway of the sample from its bottom surface at spots 2 and 4 as shown in the cartoons of Fig. 4(a), and $f_S \langle\delta T\rangle$ is the maximum temperature changing rate. Therefore, the slope of the blue curve corresponds to the propagation speed of phase boundary which is $v = 188$ $\mu\text{m/s}$ at small $L \cdot f_S \langle\delta T\rangle$. This speed is seven orders of magnitude lower than that of acoustic waves [35]. The constraint on the phase boundary propagation speed is likely related to magnetoelastic nature of the transition at T_N where the electronic degrees of freedom correlates with the lattice deformation. The formation of structural domains[36] is not directly related to the hysteresis since the domains span the whole sample along c -axis direction. However, it may be one of the reason limiting the propagation speed by causing strain and dissipating energy.

IV. CONCLUSION

Our study of thermal expansion coefficient of BaFe_2As_2 using an interferometer-based dilatometer reveals interesting information of its magnetic transition. Our results clearly resolve the two-step transition where the second-order structural transition appears at T_S and

the first-order magnetic transition at T_N . Thanks to the extremely high resolution and the "true" differential nature of our technique, we discover the samples' thickness-temperature hysteresis loop at T_N . We can describe this dynamic process with a simple model and our systematic study reveals a propagation speed of phase boundary to be $v = 188 \mu\text{m/s}$. Further understanding for the intrinsic origin of the phase boundary propagation speed needs more relevant research. This work highlights that AC-temperature dilatometry with extraordinarily high resolution is a powerful probe of correlation effects in quantum materials and it's a completely new high resolution approach for phase transition research.

ACKNOWLEDGMENTS

The work at PKU was supported by the National Key Research and Development Program of China (Grant

No. 2021YFA1401900 and 2019YFA0308403), the Innovation Program for Quantum Science and Technology (Grant No. 2021ZD0302602), and the National Natural Science Foundation of China (Grant No. 92065104 and 12074010). The work at IOP was supported by the National Key Research and Development Program of China (Grants No. 2022YFA1403400 and 2021YFA1400400), and the Strategic Priority Research Program(B) of the Chinese Academy of Sciences (Grants No. XDB33000000 and No. GJTD-2020-01). We thank Mingquan He for valuable discussion.

-
- [1] F. Hardy, N. J. Hillier, C. Meingast, D. Colson, Y. Li, N. Barišić, G. Yu, X. Zhao, M. Greven, and J. S. Schilling, Enhancement of the Critical Temperature of $\text{HgBa}_2\text{CuO}_{4+\delta}$ by Applying Uniaxial and Hydrostatic Pressure: Implications for a Universal Trend in Cuprate Superconductors, *Phys. Rev. Lett.* **105**, 167002 (2010).
- [2] M. He, X. Wang, L. Wang, F. Hardy, T. Wolf, P. Adelman, T. Bruckel, Y. Su, and C. Meingast, Uniaxial and hydrostatic pressure effects in $\alpha\text{-RuCl}_3$ single crystals via thermal-expansion measurements, *JOURNAL OF PHYSICS-CONDENSED MATTER* **30**, 385702 (2018).
- [3] R. KÜchler, P. Gegenwart, J. Custers, O. Stockert, N. Caroca-Canales, C. Geibel, J. G. Sereni, and F. Steglich, Quantum Criticality in the Cubic Heavy-Fermion System $\text{CeIn}_{3-x}\text{Sn}_x$, *Physical Review Letters* **96**, 256403 (2006).
- [4] S. Zaum, K. Grube, R. Schäfer, E. D. Bauer, J. D. Thompson, and H. v. Löhneysen, Towards the Identification of a Quantum Critical Line in the (p, B) Phase Diagram of CeCoIn_5 with Thermal-Expansion Measurements, *Phys. Rev. Lett.* **106**, 087003 (2011).
- [5] R. KÜchler, N. Oeschler, P. Gegenwart, T. Cichorek, K. Neumaier, O. Tegus, C. Geibel, J. A. Mydosh, F. Steglich, L. Zhu, and Q. Si, Divergence of the Grüneisen Ratio at Quantum Critical Points in Heavy Fermion Metals, *Physical Review Letters* **91**, 066405 (2003).
- [6] C. Meingast, F. Hardy, R. Heid, P. Adelman, A. Böhm, P. Burger, D. Ernst, R. Fromknecht, P. Schweiss, and T. Wolf, Thermal Expansion and Grüneisen Parameters of $\text{Ba}(\text{Fe}_{1-x}\text{Co}_x)_2\text{As}_2$: A Thermodynamic Quest for Quantum Criticality, *Physical Review Letters* **108**, 177004 (2012).
- [7] R. Grössinger and H. Müller, New device for determining small changes in length, *Review of Scientific Instruments* **52**, 1528 (1981).
- [8] G. O. J. B. F. Figgins and D. P. Riley, The thermal expansion of aluminium at low temperatures as measured by an X-ray diffraction method, *The Philosophical Magazine: A Journal of Theoretical Experimental and Applied Physics* **1**, 747 (1956).
- [9] Y. Gu, B. Liu, W. Hong, Z. Liu, W. Zhang, X. Ma, and S. Li, A temperature-modulated dilatometer by using a piezobender-based device, *Review of Scientific Instruments* **91**, 123901 (2020).
- [10] L. Wang, G. M. Schmiedeshoff, D. E. Graf, J.-H. Park, T. P. Murphy, S. W. Tozer, E. Palm, J. L. Sarrao, and J. C. Cooley, Application of an atomic force microscope piezocantilever for dilatometry under extreme conditions, *Measurement Science and Technology* **28**, 065006 (2017).
- [11] M. Rotter, H. Müller, E. Gratz, M. Doerr, and M. Loewenhaupt, A miniature capacitance dilatometer for thermal expansion and magnetostriction, *Review of Scientific Instruments* **69**, 2742 (1998).
- [12] R. S. Manna, B. Wolf, M. de Souza, and M. Lang, High-resolution thermal expansion measurements under helium-gas pressure, *Review of Scientific Instruments* **83**, 085111 (2012).
- [13] R. KÜchler, T. Bauer, M. Brando, and F. Steglich, A compact and miniaturized high resolution capacitance dilatometer for measuring thermal expansion and magnetostriction, *Review of Scientific Instruments* **83**, 095102 (2012).
- [14] S. Abe, F. Sasaki, T. Oonishi, D. Inoue, J. Yoshida, D. Takahashi, H. Tsujii, H. Suzuki, and K. Matsumoto, A compact capacitive dilatometer for thermal expansion and magnetostriction measurements at millikelvin temperatures, *Cryogenics* **52**, 452 (2012).
- [15] R. KÜchler, A. Wörl, P. Gegenwart, M. Berben, B. Bryant, and S. Wiedmann, The world's smallest capacitive dilatometer, for high-resolution thermal expansion and magnetostriction in high magnetic fields, *Review of Scientific Instruments* **88**, 083903 (2017).
- [16] R. KÜchler, R. Wawrzyńczak, H. Dawczak-Debicki, J. Gooth, and S. Galeski, New applications for the world's smallest high-precision capacitance dilatometer

- and its stress-implementing counterpart, *Review of Scientific Instruments* **94**, 045108 (2023).
- [17] S. O. Mariager, F. Pressacco, G. Ingold, A. Caviezel, E. Möhr-Vorobeva, P. Beaud, S. L. Johnson, C. J. Milne, E. Mancini, S. Moyerman, E. E. Fullerton, R. Feidenhans'l, C. H. Back, and C. Quitmann, Structural and Magnetic Dynamics of a Laser Induced Phase Transition in FeRh, *Phys. Rev. Lett.* **108**, 087201 (2012).
- [18] S. L. Johnson, R. A. de Souza, U. Staub, P. Beaud, E. Möhr-Vorobeva, G. Ingold, A. Caviezel, V. Scagnoli, W. F. Schlotter, J. J. Turner, O. Krupin, W.-S. Lee, Y.-D. Chuang, L. Patthey, R. G. Moore, D. Lu, M. Yi, P. S. Kirchmann, M. Trigo, P. Denes, D. Doering, Z. Hussain, Z.-X. Shen, D. Prabhakaran, and A. T. Boothroyd, Femtosecond Dynamics of the Collinear-to-Spiral Antiferromagnetic Phase Transition in CuO, *Phys. Rev. Lett.* **108**, 037203 (2012).
- [19] I. Radu, K. Vahaplar, C. Stamm, T. Kachel, N. Pontius, H. A. Dürr, T. A. Ostler, J. Barker, R. F. L. Evans, R. W. Chantrell, A. Tsukamoto, A. Itoh, A. Kirilyuk, T. Rasing, and A. V. Kimel, Transient ferromagnetic-like state mediating ultrafast reversal of antiferromagnetically coupled spins, *Nature* **472**, 205 (2011).
- [20] K. A. Seu, S. Roy, J. J. Turner, S. Park, C. M. Falco, and S. D. Kevan, Cone phase and magnetization fluctuations in Au/Co/Au thin films near the spin-reorientation transition, *Phys. Rev. B* **82**, 012404 (2010).
- [21] S. Yoshimoto, Y. Tabata, T. Waki, and H. Nakamura, Novel Slow Dynamics of Phase Transition in the Partially Ordered Frustrated Magnet DyRu₂Si₂, *Journal of the Physical Society of Japan* **92**, 094705 (2023).
- [22] Q. Huang, Y. Qiu, W. Bao, M. A. Green, J. W. Lynn, Y. C. Gasparovic, T. Wu, G. Wu, and X. H. Chen, Neutron-Diffraction Measurements of Magnetic Order and a Structural Transition in the Parent BaFe₂As₂ Compound of FeAs-Based High-Temperature Superconductors, *Phys. Rev. Lett.* **101**, 257003 (2008).
- [23] C. R. Rotundu, B. Freelon, T. R. Forrest, S. D. Wilson, P. N. Valdivia, G. Pinuellas, A. Kim, J.-W. Kim, Z. Islam, E. Bourret-Courchesne, N. E. Phillips, and R. J. Birgeneau, Heat capacity study of BaFe₂As₂: Effects of annealing, *Phys. Rev. B* **82**, 144525 (2010).
- [24] S. D. Wilson, C. R. Rotundu, Z. Yamani, P. N. Valdivia, B. Freelon, E. Bourret-Courchesne, and R. J. Birgeneau, Universal magnetic and structural behaviors in the iron arsenides, *Physical Review B* **81**, 014501 (2010).
- [25] S. D. Wilson, Z. Yamani, C. R. Rotundu, B. Freelon, E. Bourret-Courchesne, and R. J. Birgeneau, Neutron diffraction study of the magnetic and structural phase transitions in BaFe₂As₂, *Physical Review B* **79**, 184519 (2009).
- [26] M. G. Kim, R. M. Fernandes, A. Kreyssig, J. W. Kim, A. Thaler, S. L. Bud'ko, P. C. Canfield, R. J. McQueeney, J. Schmalian, and A. I. Goldman, Character of the structural and magnetic phase transitions in the parent and electron-doped BaFe₂As₂ compounds, *Phys. Rev. B* **83**, 134522 (2011).
- [27] T. R. Forrest, P. N. Valdivia, C. R. Rotundu, E. Bourret-Courchesne, and R. J. Birgeneau, The effects of post-growth annealing on the structural and magnetic properties of BaFe₂As₂, *Journal of Physics: Condensed Matter* **28**, 115702 (2016).
- [28] A. E. Böhrmer, Electronic nematic susceptibility of iron-based superconductors, *Comptes rendus. Physique (En ligne)* **17**, 90 (2016).
- [29] R. M. Fernandes, A. V. Chubukov, and J. Schmalian, What drives nematic order in iron-based superconductors? *Nature Physics* **10**, 97 (2014).
- [30] E. Gati, L. Xiang, S. L. Bud'ko, and P. C. Canfield, Role of the Fermi surface for the pressure-tuned nematic transition in the BaFe₂As₂ family, *Physical Review B* **100**, 064512 (2019).
- [31] X. Ren, L. Duan, Y. Hu, J. Li, R. Zhang, H. Luo, P. Dai, and Y. Li, Nematic Crossover in BaFe₂As₂ under Uniaxial Stress, *Phys. Rev. Lett.* **115**, 197002 (2015).
- [32] D. W. Tam, W. Wang, L. Zhang, Y. Song, R. Zhang, S. V. Carr, H. C. Walker, T. G. Perring, D. T. Adroja, and P. Dai, Weaker nematic phase connected to the first order antiferromagnetic phase transition in SrFe₂As₂ compared to BaFe₂As₂, *Physical Review B* **99**, 134519 (2019).
- [33] X. Qin, G. Cao, S. Liu, and Y. Liu, A High Resolution Dilatometer Using Optical Fiber Interferometer, (2023), [arXiv:2311.16641](https://arxiv.org/abs/2311.16641).
- [34] P. Gallo, K. Amann-Winkel, C. A. Angell, M. A. Anisimov, F. Caupin, C. Chakravarty, E. Lascaris, T. Loerting, A. Z. Panagiotopoulos, J. Russo, J. A. Sellberg, H. E. Stanley, H. Tanaka, C. Vega, L. Xu, and L. G. M. Pettersson, Water: A Tale of Two Liquids, *Chemical Reviews* **116**, 7463 (2016).
- [35] Y. Xu, N. G. Petrik, R. S. Smith, B. D. Kay, and G. A. Kimmel, Growth rate of crystalline ice and the diffusivity of supercooled water from 126 to 262 K, *Proceedings of the National Academy of Sciences* **113**, 14921 (2016).
- [36] M. A. Tanatar, A. Kreyssig, S. Nandi, N. Ni, S. L. Bud'ko, P. C. Canfield, A. I. Goldman, and R. Prozorov, Direct imaging of the structural domains in the iron pnictides aFe₂as₂ (a = Ca, Sr, Ba), *Phys. Rev. B* **79**, 180508 (2009).